Conformational and physicochemical properties of Abametapir using density functional theory

S. Dhungana*, H. S. Mallik*, T. R. Lamichhane*, S. Giri*, S. Dhungana* and H. P. Lamichhane*

*Central Department of Physics, Tribhuvan University, Kirtipur, Kathmandu, Nepal.

Abstract: Abametapir is a newly approved topical lotion for the treatment of head lice. This molecule is analyzed in the gas phase, as well as in non-polar solvent CCl_4 and polar solvent water, using Density Functional Theory with the B3LYP/6-311+G(d) exchange-correlation functional in Gaussian 16 software. The optimized molecule has two benzene rings lying in a plane with one carbon atom of each ring is replaced with a nitrogen atom. On scanning energy with respect to the vibration of dihedral angle C4–C5–C8–N9 with 10^o step in the entire dihedral angle shows the possibility of the two conformers, one of which has 99.99% occurrence at the room temperature. The FTIR, Raman and UV-visible spectra of the optimized molecule of the more stable conformer were calculated in different solvents and gaseous states. Among many modes of vibration, the bending vibration of H16-C1-H17 contributes notably to the intense FTIR signal at 1510 cm^{-1}, with a Potential Energy Distribution contribution of 52%. The highest value of Raman intensity at 1636 cm^{-1} is attributed to the stretching mode of C12-C13 (61%). The most intense peak of the UV-visible spectra of the molecule shifted from 281 nm in the gas phase to 288 nm in the CCl_4 and water solvents. Analysis of the HOMO-LUMO in different solvents and gas provided insights into the molecule's chemical stability and reactivity. This molecule has strong electrophilic behavior in both gas and solvent phases.

Keywords: Abametapir; DFT; FTIR; HOMO-LUMO; Raman.

Introduction

Head lice infestations are a widespread global health issue that imposes considerable social, psychological, and economic burdens. Traditional treatments have significantly limited their effectiveness due to the emergence of resistance, highlighting the urgent need for new medications. In this regards, 5,5′-dimethyl-2,2′-bipyridyl previously known as Ha44, the compound now identified by the name Abametapir is a metalloproteinase inhibitor designed to specifically block the activity of metalloproteinases that are pivotal for louse ova development and egg hatching[1–3]. In 2020, it received the U.S. Food and Drug Administration (FDA) approval as a topical lotion for ovicidal activity specially for the treatment of head lice in human aged six months and older. It is marketed under the trade name Xeglyze and is a pharmaceutical product. It is an organic compound with a heterocyclic product. It is an organic compound with a heterocyclic structure that can chelate to heavy metal ions such as iron, copper, and zinc. This ability allows it to interact with various targets in insects that rely on these metals as co-factors for their function, particularly metalloproteinases[4]. The chemical formula of Abametapir is $C_{12}H_{12}N_2$. Further, nitrogen-based heterocyclic pyridine derivatives are acknowledged for their therapeutic benefits, which are extensively noted for their potential as anticancer[5], antifungal[6], anti-diabetic[7] and anti-inflammatory agents[8]. There is, however, a lack of computational studies[9] on the Abametapir molecule; conducting a computational study the molecule could serve as a valuable addition to its future investigations.

This research is based on a computational approach using 311+G(d) exchange-correlation functional in Gaussian 16

Author for correspondence: Hari Shankar Mallik, Central Department of Physics, Tribhuvan University, Kirtipur, Kathmandu, Nepal.
Email: hari.mallik@cdp.tu.edu.np; https://orcid.org/0000-0001-7416-9114
Received: 3 Mar, 2025; Received in revised form: 5 Apr, 2025; Accepted: 16 April, 2025.
Doi: https://doi.org/10.3126/sw.v18i18.78689

Density Functional Theory (DFT) utilizing the B3LYP/6- software to optimize and analyze the Abametapir molecule in various solvents. After FDA approval, Abametapir seems to be a promising advancement in head lice treatment. However, this research could enhance our understanding of its long-term effects on the scalp and skin, especially regarding its absorption. Furthermore, it may provide valuable insights into the potential for resistance to Abametapir over time. The integration of this computational approach with prior experimental studies will assist future research on head lice treatment.

Materials and Methods

The preliminary structural data for Abametapir molecule was sourced from the PubChem repository[10]. The obtained molecule was subjected to geometrical optimization in the Gas and CCl_4 as well as water solvents, using Density Functional Theory (DFT) with the B3LYP/6-31+G(d) exchange-correlation functional in Gaussian 16 software[11]. An energy scan was then conducted by varying the dihedral angle of one benzene ring in the molecule to reveal the conformers. The most stable conformer was selected based on Boltzmann factor (as given in equation 1) and reoptimized with B3LYP/6-311+G(d) for further calculations in the gas phase, non-polar solvent CCl_4, and polar solvent water.

$$Boltzmann\ factor = \frac{e^{-E_i/k_BT}}{\sum_i e^{-E_i/k_BT}} \quad \ldots\ldots\ldots\ldots\ldots\ldots\ldots (1)$$

Various modes of vibration for vibrational frequency assignment and their contributions to potential energy distribution were calculated using localized symmetry in the VEDA4 software[12]. The FTIR frequency was calculated theoretically and was subsequently scaled by a factor of 0.961 to achieve the precise results[13]. The Gaussian output file from the frequency calculation in Form Check (.fch) was used to convert Raman activity into Raman intensity in the Multiwfn Analyzer, using the same scaling factor of 0.961[14]. The UV-visible absorption spectra of Abametapir were simulated using the time-dependent density functional theory (TD-DFT) approach. The simulations were conducted for the neutral state in the gas phase and also using the IEFPCM model to examine the effects of solvent behavior. The checkpoint file (.chk) of optimized geometry was used to calculate global reactivity descriptors, including HOMO-LUMO analysis.

Results and Discussion

Geometry optimization

The Abametapir molecule has 2 symmetric benzene type rings with 12 carbon, 12 hydrogen, and 2 nitrogen atoms. The molecular structure of the Abametapir is illustrated in Figure 1. The molecular geometry is optimized in the gas phase, CCl_4 and water solvent; the obtained geometric parameters are given in Table 1. To reveal all possible conformers of the Abametapir, a scan of the minimum energy configuration (potential energy surface scan) is conducted by rotating the dihedral angle C4–C5–C8–N9 in 10^o increments within the 0-360^o range for its neutral state in the gas phase, utilizing the B3LYP functional with the 6-31+G(d) basis set. The potential energy surface scan curve is depicted in Figure 2. The Figure 2 shows that there are three energy minima at the dihedral angle of -149.9° and 150.1°. Among them the molecule is more stable at 0° dihedral angle C4–C5–C8–N9. However, local minima are observed at -149.9° and 150.1° (Boltzmann factor = 0.999). The most stable conformer obtained is then reoptimized using B3LYP/6-311+G(d) for further calculations.

The structural configuration includes 27 bond lengths, of which 11 are C-C, 12 are C-H, and 4 are C-N. The bond length of C-H ranges from 1.0822 Å to 1.0946 Å and C-N from 1.3327 Å to 1.3408 Å. Similarly, C-C bond lengths are found around 1.3867 Å to 1.506 Å. The homonuclear C-C bond length is comparatively larger than that of the heteronuclear bonds C-N and C-H because of the equal electronegativity and even electron distribution between Carbons. On the other hand, nitrogen possesses larger electronegativity than that of Carbon in the C-N bond. Therefore, electrons are pulled towards the nitrogen atom leading to uneven electron density with shorter and stronger bonds forming. In C-H, the same fashion works as the Carbon atom is more electronegative than Hydrogen. The bond angles C2-C3-C4 and C11-C12-C13 are both 120.06^o

and similarly angles N9-C8-C13 and C4-C5-N6 are both 121.65º. The dihedral angle C4-C5-C8-C13 is 180º. That means two rings are in antiperiplanar form. Table 2 shows that the dipole moments of the Abametapir molecule remain

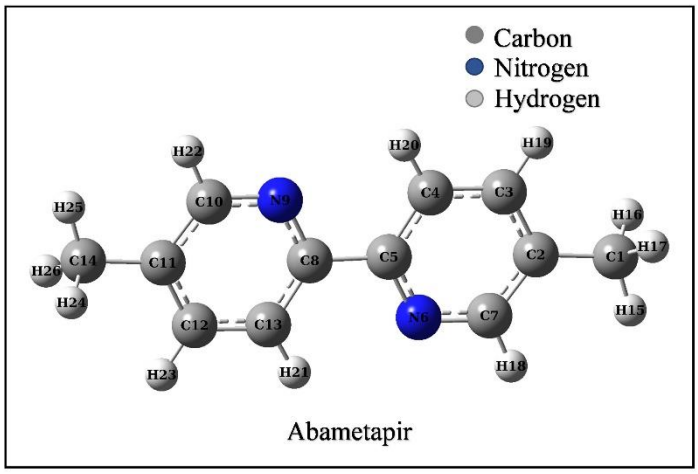

Figure 1: Optimized molecular structure of Abametapir with labeled atoms and corresponding symbols.

the same in the gas phase as in the other two solvents, regardless of whether the solvent is polar or non-polar. The total energy of the molecule is relatively low in water; thus, the compound is more stable in this solvent.

Table 1: Optimized geometrical properties such as bond lengths (Å), bond angles (º), and dihedral angles (º) of the Abametapir molecule in gas, CCl_4 and water phase.

Bonds	Gas	CCl_4	Water
	Length (Å)		
C1-C2	1.5060	1.5056	1.5053
C2-C3	1.3987	1.3988	1.3990
C3-C4	1.3867	1.3870	1.3876
C4-C5	1.4016	1.4016	1.4017
C5-N6	1.3408	1.3417	1.3430
N6-C7	1.3327	1.3338	1.3353
C2-C7	1.3978	1.3980	1.3982
C5-C8	1.4887	1.4894	1.4904
C1-H15	1.0922	1.0920	1.0917
C1-H16	1.0946	1.0944	1.0941
C1-H17	1.0946	1.0944	1.0941
C7-H18	1.0887	1.0884	1.0881
C3-H19	1.0870	1.0867	1.0863
C4-H20	1.0822	1.0819	1.0819
	Angle (º)		
C2-C1-H15	111.44	111.46	111.47
C2-C1-H16	111.46	111.36	111.24
C2-C1-H17	111.46	111.36	111.24
H15-C1-H16	107.59	107.69	107.84
H15-C1-H17	107.60	107.69	107.83
H16-C1-H17	107.08	107.06	107.02
C1-C2-C3	122.11	122.10	122.12
C1-C2-C7	121.64	121.67	121.68
C3-C2-C7	116.25	116.23	116.20
C2-C3-C4	120.06	120.04	120.04
C2-C3-H19	120.05	120.06	120.08
C4-C3-H19	119.90	119.90	119.88
C3-C4-C5	118.95	119.06	119.21
C3-C4-H20	121.75	121.55	121.15
C5-C4-H20	119.30	119.38	119.64
C4-C5-N6	121.65	121.55	121.36
C4-C5-C8	121.04	121.09	121.25
N6-C5-C8	117.31	117.37	117.39
C5-N6-C7	118.49	118.51	118.59
C2-C7-N6	124.59	124.60	124.59
C2-C7-H18	119.74	119.68	119.63
N6-C7-H18	115.68	115.72	115.77
C5-C8-N9	117.31	117.37	117.39
C5-C8-C13	121.04	121.09	121.25
	Dihedral Angle (º)		
H15-C1-C2-C3	-179.98	-179.98	-179.98
H15-C1-C2-C7	0.02	0.02	0.02
H16-C1-C2-C3	-59.76	-59.69	-59.58
H16-C1-C2-C7	120.24	120.31	120.42
H17-C1-C2-C3	59.81	59.73	59.62
H17-C1-C2-C7	-120.19	-120.27	-120.38
C1-C2-C3-C4	-180.00	-180.00	-180.00
C1-C2-C3-H19	0.00	0.00	0.00
C7-C2-C3-C4	0.00	0.00	0.00
C7-C2-C3-H19	-180.00	-180.00	-180.00
C1-C2-C7-N6	180.00	180.00	180.00
C1-C2-C7-H18	0.00	0.00	0.00
C3-C2-C7-N6	0.00	0.00	0.00
C3-C2-C7-H18	180.00	180.00	180.00

C2-C3-C4-C5	0.00	0.00	0.00
C2-C3-C4-H20	-180.00	-180.00	180.00
H19-C3-C4-C5	-180.00	180.00	180.00
H19-C3-C4-H20	0.00	0.00	0.00
C3-C4-C5-N6	0.00	0.00	0.00
C3-C4-C5-C8	-180.00	180.00	180.00
H20-C4-C5-N6	180.00	180.00	180.00
H20-C4-C5-C8	0.00	0.00	0.00
C4-C5-N6-C7	0.00	0.00	0.00
C8-C5-N6-C7	180.00	-180.00	-180.00

C4-C5-C8-N9	0.00	0.00	0.00
C4-C5-C8-C13	180.00	180.00	180.00
N6-C5-C8-N9	-180.00	180.00	180.00
N6-C5-C8-C13	0.00	0.00	0.00
C5-N6-C7-C2	0.00	0.00	0.00
C5-N6-C7-H18	180.00	-180.00	-180.00
C5-C8-N9-C10	180.00	-180.00	-180.00
C5-C8-C13-C12	-180.00	180.00	180.00
C5-C8-C13-H21	0.00	0.00	0.00

Table 2: Total energy and corresponding dipole moments of the Abametapir in its neutral state, evaluated in both the gas phase and various solvent environments.

Parameters	Neutral state		
	Gas phase	CCl_4	Water
Total energy (eV)	-15623.44	-15623.52	-15623.63
Dipole moment (Debye)	0.0001	0.0001	0.0001

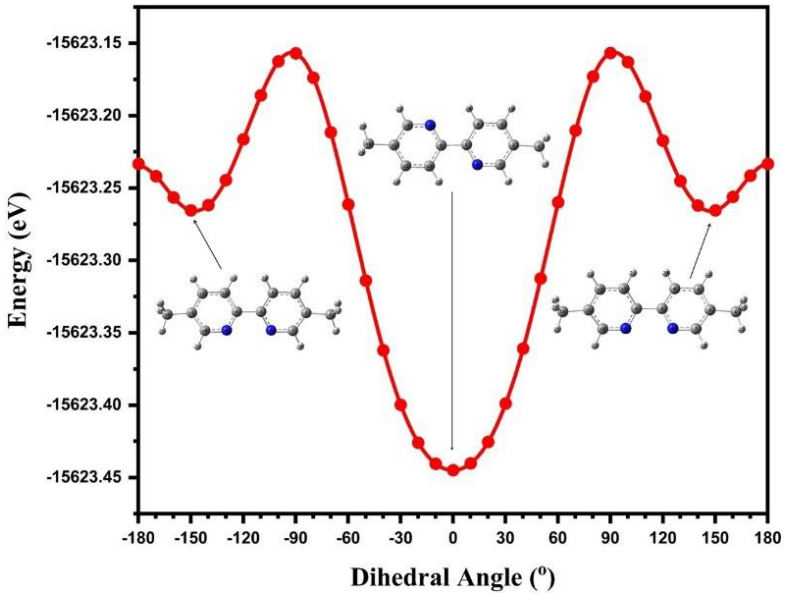

Figure 2: Potential energy surface scan of Abametapir at dihedral angle (C4–C5–C8–N9) of neutral state in the gas phase.

Vibrational assignments of intense FTIR and raman modes

Vibrational spectroscopy is capable of detecting the functional groups contained in molecules. The examined compound consists of 26 atoms and has 72 vibrational modes. These vibrational modes consist of ν-stretching, β-bending, τ-torsion, and ω-out-of-plane bending modes. The optimized configurations were utilized to determine the harmonic frequencies, infrared intensities, and Raman scattering activities, which are displayed in Table 3, highlighting only the intense FTIR and Raman modes. Figure 3 (a) and (b) summarizes the FTIR and Raman modes, respectively, in gas, CCl_4 and water solvents. The positive wavenumbers for all calculated frequencies validate the stability of the optimized structure. The vibrational modes at all frequencies, along with their potential energy distribution (PED) assignments, were computed for the neutral state in the gas phase, CCl_4 and water using VEDA software. These vibrational frequencies are scaled down by 0.961. The strongest FTIR spectral H16-C1-H17 provides a major contribution to the intense FTIR signal at 1510 cm^{-1} with the PED contribution of 52%. The peak at 3134 cm^{-1} is due to the symmetric stretching of C7-H18, predominantly contributed by potential energy

contributions. Furthermore, the stretching vibration involving C1 and H15/H16 is primarily responsible for the prominent FTIR signal at 3027 cm^{-1}. The most prominent Raman intensities are observed around 1226 to 1572 cm^{-1},

Table 3: The vibrational frequency of Abametapir, calculated at B3LYP/6-311+G(d) with PED contributions.

Mode	Gas				
	Frequency (cm^{-1})		IR intensity	Raman activity	
	Un-scaled	Scaled			Vibrational assignments (%PED)
72	3217	3092	0.00	126.79	ν(C4-H20)(98)
70	3155	3032	0.00	268.12	ν(C3-H19)(98)
69	3155	3032	48.38	0.00	ν(C3-H19)(98)
68	3134	3012	0.00	294.85	ν(C7-H18)(99)
67	3134	3012	98.29	0.00	ν(C7-H18)(99)
65	3102	2981	0.00	145.45	ν(C1-H15)80, ν(C1-H16)(19)
63	3074	2954	0.14	247.39	ν(C1-H16)99
62	3027	2909	0.00	836.47	ν(C1-H15)(19), ν(C1-H16)(81)
61	3027	2909	88.86	0.01	ν(C1-H15) (19), ν(C1-H16)(81)
59	1636	1572	0.00	1326.64	ν(C12-C13)(61), β(H21-C13-C12)(11)
56	1530	1470	0.00	461.27	ν(C2-C3)(14), β(H19-C3-C4)(17), β (H18-C7- N6)(21)
55	1513	1454	0.00	120.85	β(H24-C14-H26)(70), τ(H17-C1-C2-C3)(20)
54	1510	1451	121.77	0.00	β(H16-C1-H17)(52)
50	1432	1376	0.00	143.18	β(H15-C1-H16)(91)
48	1423	1368	0.00	100.15	ν(C2-C3)(10), ν(C5-C8)(17), β(H21-C13-C12)(10), β(C1-C2-C7)(12)
45	1327	1275	0.00	256.95	ν(C5-C8)(33), β(H19-C3-C4)(30)
42	1276	1226	0.00	325.87	ν(N6-C5)(70)
41	1246	1198	0.00	123.61	ν(C2-C3)(12), ν(C11-C14)(49), β (H19-C3-C4)(13)
38	1155	1110	0.00	58.09	ν(C12-C13)(16), β(H21-C13-C12)(64)
25	848	815	59.90	0.00	τ(H19-C3-C2-C1)(86)
	CCl_4				
72	3219	3093	0.00	200.28	ν(C4-H20) (98)
70	3159	3036	0.00	389.12	ν(C3-H19) (98)
69	3159	3036	55.36	0.00	ν(C3-H19) (98)
68	3137	3015	0.00	423.02	ν(C7-H18) (99)
67	3137	3015	117.98	0.00	ν(C7-H18) (99)
65	3104	2983	0.00	218.40	ν(C1-H15) (80), ν(C1-H16) (20)
63	3076	2956	0.12	338.74	ν(C1-H16) (99)
62	3029	2911	0.00	1143.65	ν(C1-H15) (20), ν(C1-H16) (80)
61	3029	2911	96.98	0.02	ν(C1-H15) (20), ν(C1-H16) (80)
59	1634	1570	0.00	2207.87	ν(C3-C4) (59)
56	1529	1469	0.00	814.15	ν(N9-C8) (21), ν(C1-C2) (10), ν(C1-C2) (11), β(H19-C3-C4) (17), β(H22-C10-N9) (19)
55	1508	1449	177.43	0.00	β(H20-C4-C5) (55)
54	1508	1449	0.00	198.25	β(H16-C1-H17) (-56), τ(H24-C14-C11-C10) (23)
50	1429	1373	0.00	227.25	β(H16-C1-H17) (68)
48	1421	1366	0.00	151.38	ν(C2-C3) (17), β(H21-C13-C12) (-11), β(C1-C2-C7) (11)
45	1325	1273	0.00	445.18	ν(C5-C8) (31), β(H19-C3-C4) (30)
42	1275	1225	0.00	542.89	ν(C5-C8) (77)
41	1246	1197	0.00	230.22	ν(C1-C2) (59), β(H19-C3-C4) (14)
38	1153	1108	0.00	96.82	ν(C3-C4) (11), β(H21-C13-C12) (64)
25	848	815	71.97	0.00	τ(H20-C4-C5-C8) (82)
	Water				
72	3220	3094	0.00	405.77	ν(C4-H20) (98)
70	3167	3044	0.00	590.85	ν(C3-H19) (98)

69	3167	3043	62.96	0.00	ν(C3-H19) (98)
68	3142	3020	0.00	618.33	ν(C7-H18) (99)
67	3142	3019	139.82	0.00	ν(C7-H18) (99)
65	3108	2987	62.22	7.18	ν(C1-H16) (15), ν(C1-H15) (80)
63	3080	2960	0.02	493.72	ν(C1-H17) (75)
62	3032	2914	0.00	1602.33	ν(C1-H16) (60), ν(C1-H15) (20)
61	3032	2914	104.77	0.00	ν(C1-H15) (20), ν(C14-H24) (60)
59	1632	1568	0.00	3729.78	ν(C2-C7) (-59), β(H19-C3-C4) (10)
56	1527	1468	0.00	1476.94	ν(N6-C5) (14), ν(C1-C2) (16), β(H19-C3-C4) (19), β(H18-C7-N6) (23)
55	1506	1447	244.14	0.00	ν(N9-C8) (12), β(H18-C7-N6) (52)
54	1503	1444	0.00	321.73	β(H15-C1-H16) (69), τ(H16-C1-C2-C3) (20)
50	1426	1371	0.00	395.66	β(H15-C1-H16) (86)
48	1419	1363	0.00	227.41	ν(C2-C3) (12), β(C11-C12-C13) (10), β(C1-C2-C7) (11)
45	1324	1272	0.00	801.03	ν(C2-C3) (36), β(H19-C3-C4) (23)
42	1273	1224	0.00	894.64	ν(C2-C3) (72)
41	1245	1197	0.00	474.25	ν(C1-C2) (65), β(H19-C3-C4) (12)
38	1152	1107	0.00	190.87	ν(C2-C7) (20), β(H19-C3-C4) (62)
25	846	813	102.26	0.00	τ(H19-C3-C2-C1) (85)

scaling factor: 0.961; ν: stretching; β: bending; τ: torsion; ω: out-of-plane bending modes

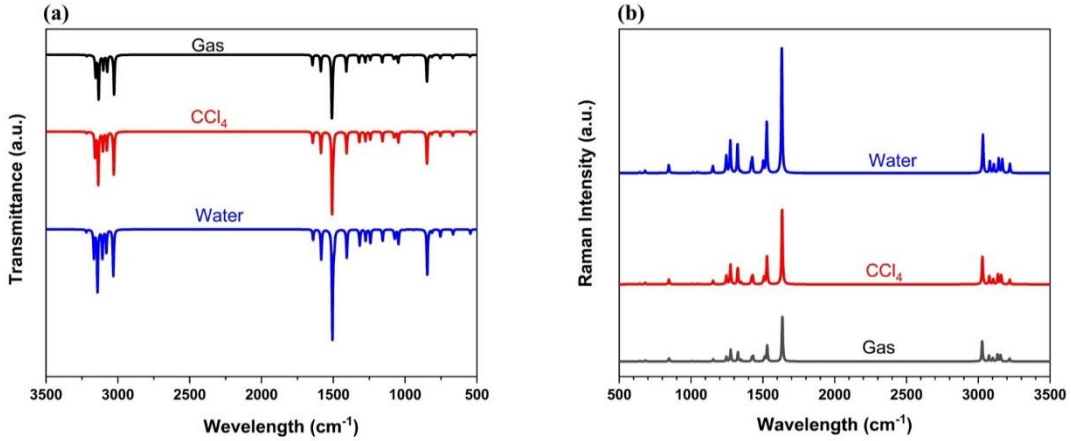

Figure 3: a) FTIR and b) Raman spectrum: A comparison of different modes of Abametapir molecule in gas, CCl_4 and water.

with the extremely intense peak at 1572 cm^{-1} due to the stretching mode of C12-C13 (61%) and bending mode of H21-C13-C12 (11%). Similarly, other intense peaks are observed at 1470 cm^{-1} with a Raman intensity of 407.46, and at 1226 cm^{-1} with a Raman intensity of 377.38, due to the stretching mode of N6-C5 with potential energy contribution 70%. There is no significant difference is observed in other two solvents.

C-H vibration: The C-H stretching modes, observed in the range of approximately 2850 to 3000 cm^{-1}, have been documented in earlier reports[15]. The molecular spectral bands and PED contribution values are 3092(98%), 3032(98%), 3012(99%), 2981(80%), 2954(99%), 2909(81%) cm^{-1}. There is no pure stretching vibration observed in any case and also there is no significant difference is observed in other two solvents.

C-N vibration: The nitrogen-carbon N-C vibration is found in the range of 1400 to 1200 cm^{-1}, appearing as a mixed band[13]. N-C vibrations of the title compound are detected at 1355(30%), 1270(45%), 1228(63%), 1226(70%) cm^{-1}. In the gas phase and no significant difference is observed in other two solvents.

C-C vibration: The C-C stretching vibration is expected to occur within the range of 800 to 1650 cm^{-1} [16]. C-C stretching vibration are observed at 1581(60%), 1572(61%), 1553(46%), 1525(48%), 1470(14%), 1368(10%), 1297(25%), 1275(33%), 1198(12%), 1194(57%), 1110(16%), 1037(19%), 814(44%), 781(61%),656(20%),

274(43%) cm^{-1} in the gas phase and no significant difference is observed in other two solvents.

UV-vis absorption spectra

UV absorption of the title molecule is theoretically calculated using TD-DFT (Time Dependent DFT) approach. The computed properties, including maximum absorption wavelengths (λ), excitation energies (E) and oscillator strengths(*f*) are summarized in Table 4. For the title molecule, the theoretical electronic absorption wavelengths are 281 nm in the gas phase, 288 nm in CCl_4, and 288 nm in water, which are depicted in Figure 4. It is observed that the most intense peak of the UV-visible spectra of the molecule shifted from 281 nm in the gas phase to 288 nm in the CCl_4 and water solvents.

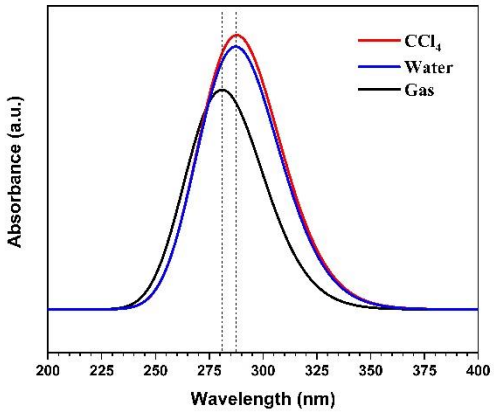

Figure 4: The electronic transition states of Abametapir using TD-DFT methods.

Frontier molecular orbital

Frontier molecular orbitals play an important role in optical and electrical properties. The calculation of the global reactivity descriptor is crucial in DFT because these values can be used to comprehend the links between a molecule's structure, stability, and reactivity[17]. Light absorption leads to an electron transition from the HOMO (Highest Occupied Molecular Orbital) to the LUMO (Lowest Unoccupied Molecular Orbital)[18]. Molecules with a larger energy gap are good indicators of chemical hardness, while those with a smaller energy gap are considered soft molecules. As a result, a hard molecule requires more energy to excite an electron from the HOMO to the LUMO orbital[19]. Electronegativity (χ) indicates how strongly a molecule attracts electrons. The electrophilicity index(ω) measures the extent to which a molecule possesses electrophilic properties. The following global reactivity descriptors[20] are calculated for charge transfer interaction using HOMO-LUMO energy in the present paper:

$\text{Ionization Potential(IP)} = -E_{HOMO};$

$\text{Electron Affinity(EA)} = -E_{LUMO};$

$\text{Energy Gap}(\Delta E_g) = \text{IP} - \text{EA};$

$\text{Electronegativity}(\chi) = \frac{1}{2}(\text{EA} + \text{IP});$

$\text{Chemical Hardness}(\eta) = \frac{1}{2}(\text{IP} - \text{EA});$

$\text{Chemical Softness}(\zeta) = \frac{1}{\eta}$

$\text{Chemical Potential}(\mu) = -\frac{\text{EA+IP}}{2};$

$\text{Electrophilic Index}(\omega) = \frac{\mu^2}{2\eta}$

The frontier molecular orbitals, specifically the HOMO and LUMO, are calculated using DFT with the 6-311+G(d) basis set for the neutral singlet state in both gas phase and various solvents, including non-polar solvent CCl_4 and polar solvent water. This analysis is conducted to compare the effects of different polar and nonpolar solvents in the IEFPCM model. The red and green colors in the orbital figure of the molecule (see Figure 5) correspond to negative and positive phases respectively. The energy gap of the compound in the gas phase is 4.788 eV. In other solvents, the energy gaps are 4.779 eV in CCl_4 and 4.763 eV in Water. This is consistent with the UV-Vis spectra of the molecule. The electrophilicity index (ω), categorizes organic compounds into three groups[21]: strong electrophiles with $\omega > 1.5$ eV, moderate electrophiles with $0.8 < \omega < 1.5$ eV, and marginal electrophiles with $\omega < 0.8$ eV. The title compound demonstrates strong electrophilic behavior in both the gas phase and solvent phase in its singlet state, as its value is nearly above 3 eV.

Conclusions

A computational study has been undertaken to examine the structural and spectral characteristics of the 5,5′-dimethyl-2,2′-bipyridyl (Abametapir) molecule. The molecule has

Table 4: Theoretical analysis of electronic transition states of Abametapir using TD-DFT methods.

	Neutral state		
Parameters	Gas phase	CCl_4	Water
Absorption Wavelength (nm)	281	288	288
Oscillator Strength (*f*)	0.002	0.003	0.745
Excitation Energy (eV)	4.2464	4.2762	4.3158
Major contribution	H-1→L(70.0%)	H-1→L(70.0%)	H→L(69.3%)
Symmetry	singlet-A	singlet-A	singlet-A

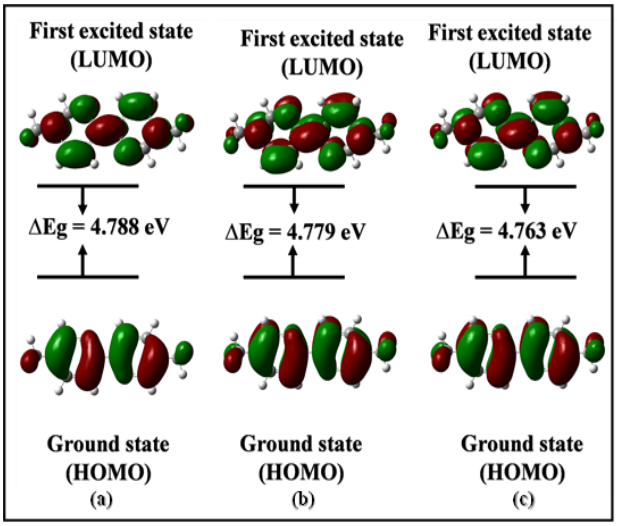

Figure 5: Spatial distribution of atomic orbitals in the frontier molecular orbitals (FMOs) of the title compound in various solvent phases (a) gas (b) CCl_4 and (c) water.

Table 5: Global reactivity parameters and molecular orbital energies of the Abametapir.

Parameters	Solvent		
	Gas	CCl_4	Water
E_{HOMO} (eV)	-6.3403	-6.4045	-6.5185
E_{LUMO} (eV)	-1.5519	-1.6259	-1.7551
Energy gap (eV)	4.7884	4.7786	4.7634
Ionization potential (eV)	6.3403	6.4045	6.5185
Electron Affinity (eV)	1.5519	1.6259	1.7551
Chemical potential (eV)	-3.9461	-4.0152	-4.1368
Electronegativity (eV)	3.9461	4.0152	4.1368
Chemical Hardness (eV)	2.3942	2.3893	2.3817
Chemical softness $(eV)^{-1}$	0.4177	0.4185	0.4199
Electrophilicity index (eV)	3.2519	3.3737	3.5927

-2,2′-bipyridyl (Abametapir) molecule. The molecule has only one most stable structure at room temperature. It is optimized in the gas phase, a non-polar solvent, and a polar solvent to assess the effects. There are no significant changes in FTIR and Raman modes across all three cases; however, notable changes are observed in the UV-vis spectra for the gas phase and solvent phase, while no changes occur in both non-polar and polar solvents, CCl_4 and water, respectively. Analysis of the HOMO-LUMO in various solvents and gas provided insights into the molecule's chemical stability and reactivity. This analysis also indicates that the molecule is more stable in water at room temperature, along with optimized parameters. This study will further be useful for molecular docking to explore new possibilities for the use of the Abametapir molecule.

Acknowledgements

The authors would like to thank Prof. Dr. Rajendra Parajuli and Asst. Prof. Pitambar Shrestha from Amrit Science College, Tribhuvan University, Thamel, Kathmandu, Nepal for providing access to Gaussian calculations.

References

[1] Van Hiel, M. B. et al. 2012.The ovicidal, larvacidal and adulticidal properties of 5,5′-dimethyl-2,2′-bipyridyl against *Drosophila melanogaster*. Smagghe G, ed. *PLoS ONE*. **7**(11): e49961. Doi: 10.1371/journal.pone.0049961

[2] Bowles, V. M. et al. 2018. Clinical studies evaluating abametapir lotion, 0.74%, for the treatment of head louse infestation. *Pediatric Dermatology*. **35**(5): 616-621. Doi: 10.1111/pde.13612

[3] Taylor, S., Walther, D., Fernando, D. D., Swe-Kay, P. and Fischer ,K. 2022.Investigating the antibacterial properties of prospective scabicides. *Biomedicines*. **10**(12): 3287. Doi: 10.3390-/biomedicines10123287

[4] Bowles, V. M., Yoon, K. S., Barker, S. C., Tran, C., Rhodes, C. and Clark, M. J. 2017. Ovicidal efficacy of abametapir against eggs of human head and body lice (Anoplura: Pediculidae). *J Med Entomol*. **54**(1): 167-172. Doi: 10.1093/jme/tjw132

[5] Mohamed , E. A., Ismail, NSM., Hagras, M. and Refaat, H. 2021. Medicinal attributes of pyridine scaffold as anticancer targeting

agents. *Futur J Pharm Sci*. 2021. **7**(1): 24.
Doi: 10.1186/s43094-020-00165-4

[6] Mashaly, M. M., Abd-Elwahab, Z. H. and Faheim, A. A. 2004. Preparation, spectral characterization and antimicrobial activities of schiff base Complexes Derived from 4-Aminoantipyrine. Mixed Ligand Complexes with 2-Aminopyridine, 8-Hydroxyquinoline and Oxalic Acid and Their Pyrolytical Products. *J Chinese Chemical Soc*. **51**(5A): 901-915.
Doi: 10.1002/jccs.200400135

[7] Chandran, E. A., Vineesha, M. & Valooran, N. M., 2023. A. Kumar R. A Recent Update on Pyridine Derivatives as a Potential Lead for Diabetes Mellitus. J. *Chem. Rev*. **5**(2): 159-182.
Doi: https://doi.org/10.22034/JCR.366462.1198

[8] Ali, E. MH. et al.2021. Design, synthesis and anti-inflammatory activity of imidazol-5-yl pyridine derivatives as p38α/MAPK14 inhibitor. *Bioorganic & Medicinal Chemistry*. **31**: 115969.
Doi: 10.1016/j.bmc.2020.115969

[9] Rifana, B. A.2024. Optimized structure, spectroscopy research, reactive site analysis and pharmaceutical studies on abametapir – a DFT approach. *Acta Scientific Pharmaceutical Sciences*. **8**(7): 61-67.

[10] PubChem. abametapir. Accessed February 19, 2025.
Doi: https://pubchem.ncbi.nlm.nih.gov/compound/15664

[11] Frisch, M. J. et al.2016. Gaussian˜16 Revision C.01. Published online 2016.

[12] Jamróz, M. H.2013. Vibrational energy distribution analysis (veda): scopes and limitations. *Spectrochimica Acta Part A: Molecular and Biomolecular Spectroscopy*. **114**: 220-230.
Doi: 10.1016/j.saa.2013.05.096

[13] Saral, A., Sudha, P., Muthu, S., Sevvanthi, S., Sangeetha, P. and Selvakumari, S. 2021. Vibrational spectroscopy, quantum computational and molecular docking studies on 2-chloroquinoline-3-carboxaldehyde. *Heliyon*. **7**(7): e07529.
Doi: 10.1016/j.heliyon.2021.e07529

[14] Liu, Z., Lu, T. and Chen, Q. 2021. Vibrational spectra and molecular vibrational behaviors of all-carboatomic rings, cyclo[18]carbon and. its analogues. *Chemistry An Asian Journal*. **16**(1): 56-63.
Doi: 10.1002/asia.202001228

[15] Ghalla, H., Issaoui, N., Govindarajan, M., Flakus, H.T., Jamroz, M. H. and Oujia, B. 2014. Spectroscopic and molecular structure investigation of 2-furanacrylic acid monomer and dimer using HF and DFT methods. *Journal of Molecular Structure*. **1059**: 132-143.
Doi: 10.1016/j.molstruc.2013.11.037

[16] Nirmala, T. et al. 2024. Spectroscopic, molecular structure electronic topology surface and pharmaceutical investigation of 1-[(4-Chlorophenyl) methyl]-1H-indole-3-carboxaldehyde by quantum computation-Prediction of antitumor activity. *Chemical Physics Impact*. **8**: 100513.
Doi: 10.1016/j.chphi.2024.100513

[17] Pratiwi, R., Ibrahim, S. and Tjahjono, D. H. 2020. Reactivity and stability of metalloporphyrin complex formation: dft and experimental study. *Molecules*. **25**(18): 4221.
Doi: 10.3390/molecules25184221

[18] Deghady, A. M., Hussein, R. K., Alhamzani, A. G. and Mera ,A. 2021. Density functional theory and molecular docking investigations of the chemical and antibacterial activities for 1-(4-hydroxyphenyl)-3-phenylprop-2-en-1-one. *Molecules*. **26**(12): 3631.
Doi: 10.3390/molecules26123631

[19] Adejumo, T. T. et al. 2020. Synthesis, characterization, catalytic activity, and dft calculations of zn(ii) hydrazone complexes. *Molecules*. **25**(18**)**: 4043.
Doi: 10.3390/molecules25184043

[20] Rijal, R. et al. 2022. Quantum chemical calculations of nicotine and caffeine molecule in gas phase and solvent using DFT methods. *Heliyon*. **8**(12): e12494.
Doi: 10.1016/j.heliyon.2022.e12494

[21] Domingo, L. R., Ríos-Gutiérrez, M. and Pérez, P. 2016. Applications of the conceptual density functional theory indices to organic chemistry reactivity. *Molecules*. **21**(6): 748.
Doi: 10.3390/molecules21060748